Inorganic Chemistry

pubs.acs.org/IC
Article

Synergism of Holmium Orthovanadate/Phosphorus-Doped Carbon Nitride Nanocomposite: Nonenzymatic Electrochemical Detection of Hydrogen Peroxide

Thangavelu Kokulnathan, Tzyy-Jiann Wang,* Faheem Ahmed, Thamraa Alshahrani, and Nishat Arshi

Cite This: *Inorg. Chem.* 2024, 63, 3019−3027
Read Online

ABSTRACT: Developing efficient and robust electrode materials for electrochemical sensors is critical for real-time analysis. In this paper, a hierarchical holmium vanadate/phosphorus-doped graphitic carbon nitride ($HoVO_4$/P-CN) nanocomposite is synthesized and used as an electrode material for electrochemical detection of hydrogen peroxide (H_2O_2). The $HoVO_4$/P-CN nanocomposite exhibits superior electrocatalytic activity at a peak potential of −0.412 V toward H_2O_2 reduction in alkaline electrolytes while compared with other reported electrocatalysts. The $HoVO_4$/P-CN electrochemical platform operated under the optimized conditions shows excellent analytical performance for H_2O_2 detection with a linear concentration range of 0.009−77.4 μM, a high sensitivity of 0.72 μA μM^{-1} cm^{-2}, and a low detection limit of 3.0 nM. Furthermore, the $HoVO_4$/P-CN-modified electrode exhibits high selectivity, remarkable stability, good repeatability, and satisfactory reproducibility in detecting H_2O_2. Its superior performance can be attributed to a large specific surface area, high conductivity, more active surface sites, unique structure, and synergistic action of $HoVO_4$ and P-CN to benefit enhanced electrochemical activity. The proposed $HoVO_4$/P-CN electrochemical platform is effectively applied to ascertain the quantity of H_2O_2 in food and biological samples. This work outlines a promising and effectual strategy for the sensitive electrochemical detection of H_2O_2 in real-world samples.

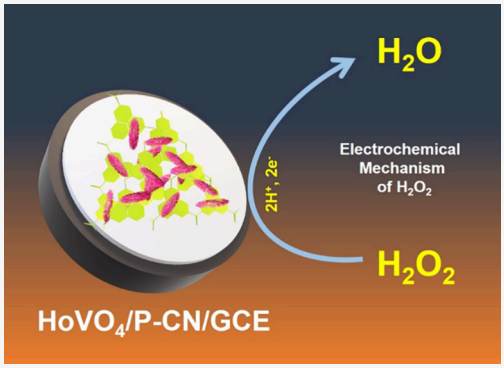

1. INTRODUCTION

Hydrogen peroxide (H_2O_2) is an essential member of stable reactive oxygen species and volatile inorganic compounds with strong oxidizing characteristics.[1−3] It has been widely deployed in chemical industries, textiles, healthcare, fuel cells, food processing, and water treatments.[4−6] Notably, low-concentration H_2O_2 (3−6%) is imperative in the coronavirus disease 2019 pandemic as a curative disinfectant to disinfect object surfaces, confined air, skin injury, and medical devices.[7] In many countries, H_2O_2 is used in sterilizing milk and milk product packaging to preserve them.[8] The annual H_2O_2 production exceeds 4 billion tons, and its global demand is expected to reach about 6 billion tons by 2024.[9] Regular doses under the acceptable range did not have adverse effects. However, the excessive level of H_2O_2 may cause Alzheimer's disease, Parkinson's disease, diabetic nephropathy, cardiovascular diseases, cell carcinogenesis, DNA damage, neurodegeneration, malignancies, arteriosclerosis, and cancers.[10−14]

The improper discharge of H_2O_2 and its residues from various industrial sectors without proper treatment leads to serious environmental problems. Due to such toxicity, the U.S. Food and Drug Administration limits H_2O_2 residuals in packaging commodities below 0.5 ppm.[15] The Chinese Food Sanitation Act prohibits H_2O_2 residues in foodstuffs and health products.[16] Unfortunately, overuse, residue, and illegal addition of H_2O_2 occur frequently in many countries. For this reason, it is essential to accurately inspect the concentration level of H_2O_2 in food and biological samples.

Various analytical approaches are developed in detecting H_2O_2, which include surface-enhanced Raman spectroscopy, electrochemical detection, molecularly imprinted sensors, enzyme-linked immunoassay, photoluminescence, photoelectrochemical sensors, colorimetric detection, mass spectrometry, high-performance liquid chromatography, and colorimetric detection.[17−23] Among these, electrochemical detection has drawn tremendous attention due to its fast response, high sensitivity, portability, high reliability, better accuracy, miniaturization, low cost, and user-friendly approach.[24−29] Electrode materials are vital in electrochemical analysis to achieve an enhanced and high electrochemical performance. Kaplan et al. fabricated a nonenzymatic electrochemical sensor

Received: October 28, 2023
Revised: January 5, 2024
Accepted: January 5, 2024
Published: January 29, 2024

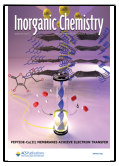

https://doi.org/10.1021/acs.inorgchem.3c03804
Inorg. Chem. 2024, 63, 3019−3027

Scheme 1. Schematic Diagram for the Preparation of the $HoVO_4$/P-CN Nanocomposite

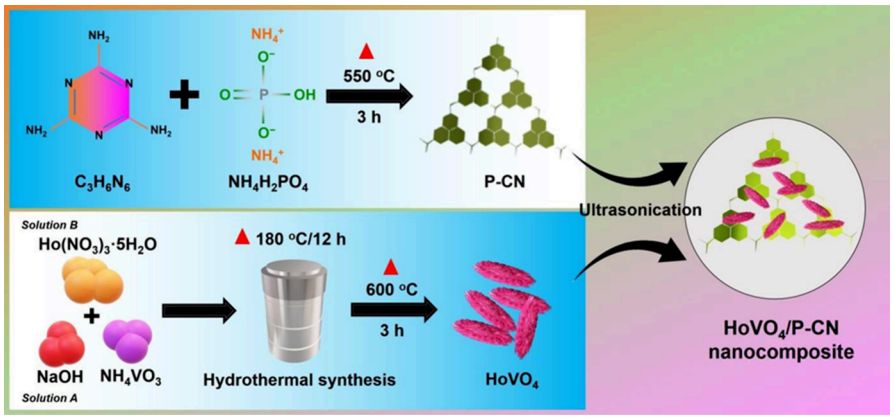

based on nickel−iron oxide@sulfur-doped reduced graphene oxide modified glassy carbon electrodes (GCEs) to detect H_2O_2.[30] Xiong et al. synthesized cobalt oxide nanoparticles/porous carbon nanobox nanocomposites and used them as an electrode material for nonenzymatic electrochemical H_2O_2 detection.[31] Therefore, the development of efficient electrode materials to enhance electrochemical performance for H_2O_2 detection is paramount.

Many research efforts have been directed toward the advancement of robust electrode constituents with markedly proficient electrocatalytic behavior tailored for use in electrochemical sensors. As electrode materials, binary metal oxides possess several advantages for electrochemical sensors over single-metal oxides as they have multiple oxidation states and high electrical conductivity.[32] In line with the above, rare-earth orthovanadates have stimulated remarkable research interest for prospective electrode materials in electrochemical applications due to their remarkable physicochemical properties.[33−36] Notably, holmium orthovanadate ($HoVO_4$) is recognized as one capable electrode constituent possessing characteristics well suited for electrochemical sensors, such as high surface area, multiple exposed active sites, high electrical conductivity, adjustable structures, and tunable electronic structure, to show excellent electrocatalytic performance.[37,38] These unique properties make it a high-performance electrode material and an ideal electrochemical platform for studying the structure−performance relationship during the electrocatalytic process. Sriram et al. prepared the $HoVO_4$/f-boron nitride nanocomposite through an ultrasonication method to achieve efficient electrochemical sensing toward mercury ions.[39] Although pristine $HoVO_4$ has several advantages for electrochemical sensors, its low mass transfer efficiency and limited electrochemical stability are significant limitations. Therefore, to avoid these hindrances, coupling the pristine $HoVO_4$ with a conductive matrix can be adopted as a valuable strategy to enhance the electrochemical properties.

Specifically, graphitic carbon nitride (g-C_3N_4, labeled g-CN) with a two-dimensional layered structure exhibits versatile redox properties and high durability and has been widely studied for electrochemical sensors.[40−43] Additionally, incorporating heteroatoms into the structural framework of g-CN can considerably develop the catalytic performance of the electrochemical sensor by enhancing electron conductivity, charge distribution, desirable electronic structure, open edge sites, lattice defects, remarkable mechanical robustness, multiple chemical properties, and ample charge transportation.[44−47] Phosphorus can be doped into the g-CN lattice (P-CN) for tuning physiochemical properties and enhancing electrocatalytic efficiency.[48] Ahmed et al. synthesized zinc oxide/P-CN composites for electrochemical detection of nitrofurantoin, which was proven to be an efficient electrode material with good electrochemical performance.[49] Sriram et al. reported that manganese cobalt oxide encapsulated a P-CN-modified electrode for sulfadiazine detection with high sensitivity.[50]

Inspired by the aforementioned considerations, we synthesized the $HoVO_4$/P-CN nanocomposite through hydrothermal and sonochemical methods for electrochemical detection. To the best of our knowledge, this is the first report on the design and construction of $HoVO_4$/P-CN nanocomposite-based electrode material applied in the nonenzymatic electrochemical H_2O_2 sensors. The prepared $HoVO_4$/P-CN nanocomposite is methodically investigated and characterized by using several analytical techniques. The studies on cyclic voltammograms (CV) for H_2O_2 detection confirm that the $HoVO_4$/P-CN nanocomposite-modified GCE has better electrochemical performance than the pristine $HoVO_4$/GCE and P-CN/GCE due to enhanced electroactive sites, synergistic effect, fast electron/mass transfer, high conductivity, and large surface area. This excellent electrochemical performance of $HoVO_4$/P-CN/GCE includes a broad detection range, low limit of detection (LOD), high steady-state stability, good selectivity, high sensitivity, and good reproducibility and repeatability. Moreover, the $HoVO_4$/P-CN-based electrochemical sensor is effectually utilized for determining the H_2O_2 quantity in actual samples. This study provides a new perspective for constructing rare-earth orthovanadate-based electrode materials with hierarchical nanostructures for high-efficiency electrochemical sensors.

2. EXPERIMENTAL SECTION

Materials, instrumentation, and synthesis of $HoVO_4$ nanorices and P-CN nanosheets are listed in the Supporting Information.

2.1. Preparation of the $HoVO_4$/P-CN Nanocomposite. The $HoVO_4$/P-CN nanocomposite was prepared by using the ultrasonic method. First, 15 mg of $HoVO_4$ and 10 mg of P-CN were dispersed in 10 mL of DI water by ultrasonication for 60 min. The obtained material was centrifuged, rinsed with DI water several times, and finally dried overnight to acquire the $HoVO_4$/P-CN nanocomposite. The synthesis process of the $HoVO_4$/P-CN nanocomposite is schematically shown in Scheme 1.

2.2. Electrode Modification by $HoVO_4$, P-CN, and $HoVO_4$/P-CN. Before modification, the bare GCE was polished by an aqueous

https://doi.org/10.1021/acs.inorgchem.3c03804
Inorg. Chem. 2024, 63, 3019−3027

slurry of alumina powder with a 0.5 μm average particle size. Then, it was thoroughly rinsed in DI water and dried in air. The electrocatalyst solution was prepared by dispersing 5 mg of the $HoVO_4$/P-CN nanocomposite into 1 mL of DI water under ultrasonication for 15 min to form a homogeneous suspension. Afterward, 8.0 μL of the $HoVO_4$/P-CN suspension was dropped onto the surface of the pretreated GCE and dried in air. The same process was used to construct other modified electrodes, including $HoVO_4$/GCE and P-CN/GCE, for comparison.

2.4. Safety Statement. No uncommon hazards are noted.

3. RESULT AND DISCUSSION

3.1. Physical Characterization. The synthesized P-CN, $HoVO_4$, and $HoVO_4$/P-CN nanocomposites were examined through a series of characterization methods. The crystallographic structure of $HoVO_4$, P-CN, and $HoVO_4$/P-CN was analyzed by the X-ray diffraction (XRD) technique, as depicted in Figure 1A. The diffraction peak at a 2θ value of 24.7° in

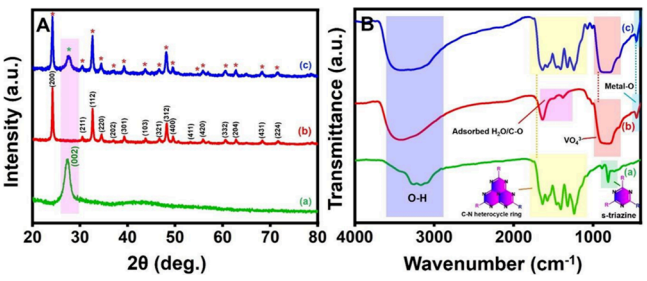

Figure 1. (A) XRD patterns and (B) FTIR spectra of the (a) P-CN, (b) $HoVO_4$, and (c) $HoVO_4$/P-CN nanocomposite.

Figure 1A(a) is assigned to the (0 0 2) lattice plane of P-CN, which is in agreement with the literature.[49] The formation of this structure can increase the interlayer spacing of P-doped CN, which could provide more active sites and surface irregularities to improve electrochemical activity.[50] In addition, it increases the density of the states closer to the Fermi level, improves conductivity, and facilitates the charge transfer at the electrode/electrolyte interface. In Figure 1A(b), the diffraction peaks at 24.2, 30.4, 32.6, 34.4, 37.0, 39.2, 43.7, 46.6, 48.1, 49.5, 53.2, 55.8, 60.5, 62.7, 68.2, and 71.6° are assigned to the (2 0 0), (2 1 1), (1 1 2), (2 2 0), (2 0 2), (3 0 1), (1 0 3), (3 2 1), (3 1 2), (4 0 0), (4 1 1), (4 2 0), (3 3 2), (2 0 4), (4 3 1), and (2 2 4) lattice planes of tetragonal $HoVO_4$, respectively, according to the JCPDS card no. 34-0421 of $HoVO_4$.[39] The XRD pattern of the $HoVO_4$/P-CN nanocomposite in Figure 1A(c) displays every diffraction peak of $HoVO_4$ and P-CN, confirming the successful loading of $HoVO_4$ on the surface of P-CN without hampering its original structure. The absence of any impurity peaks in Figure 1A(c) demonstrates the formation of a high-purity $HoVO_4$/P-CN nanocomposite. Such results show the efficacious formation of the $HoVO_4$/P-CN nanocomposite.

Fourier transform infrared (FTIR) spectroscopy is employed to analyze the surface functional groups of the as-prepared samples, and related outcomes are depicted in Figure 1B. In Figure 1B(a), the characteristic absorption peaks at 1200−1600 cm^{-1} are attributed to the stretching vibration modes of CN heterocycles in the P-CN. The sharp absorption peak at 810 cm^{-1} is accredited to the out-of-plane breathing vibration of tri-*s*-triazine units in CN heterocycles.[47] The wide absorption peak at 3000−3500 cm^{-1} is ascribed to its residual N−H component and O−H band, which are allied with uncondensed amino groups and surface-adsorbed water molecules.[49] Notably, no vibration or stretching modes related to the P element are observed owing to the overlapping of the C−N bond vibration. For $HoVO_4$, strong peaks at 830 and 455 cm^{-1} in Figure 1B(b) are attributed to the V−O (from the VO_4^{3-} group) and the M−O stretching vibration. The weak peaks located at 3423 and 1637 cm^{-1} are ascribed to the bending vibration of water molecules. In Figure 1B(c), all the main characteristic peaks of $HoVO_4$ and P-CN are well present in the FTIR spectrum of the $HoVO_4$/P-CN nanocomposite, obviously confirming the successful formation of the $HoVO_4$/P-CN nanocomposite, which is in agreement with the XRD characterization results.

X-ray photoelectron spectroscopy (XPS) is used to analyze the surface chemical compositions and the valence states of the $HoVO_4$/P-CN nanocomposite. The XPS survey spectrum in Figure S1 reveals the presence of Ho 4d, V 2p, O 1s, C 1s, N 1s, and P 2p elements on the surface of the $HoVO_4$/P-CN nanocomposite. The high-resolution XPS spectrum of Ho 4d in Figure 2A demonstrates two peaks at 162.4 and 158.5 eV, which are assigned to Ho $4d_{3/2}$ and Ho $4d_{5/2}$, respectively.[39] In

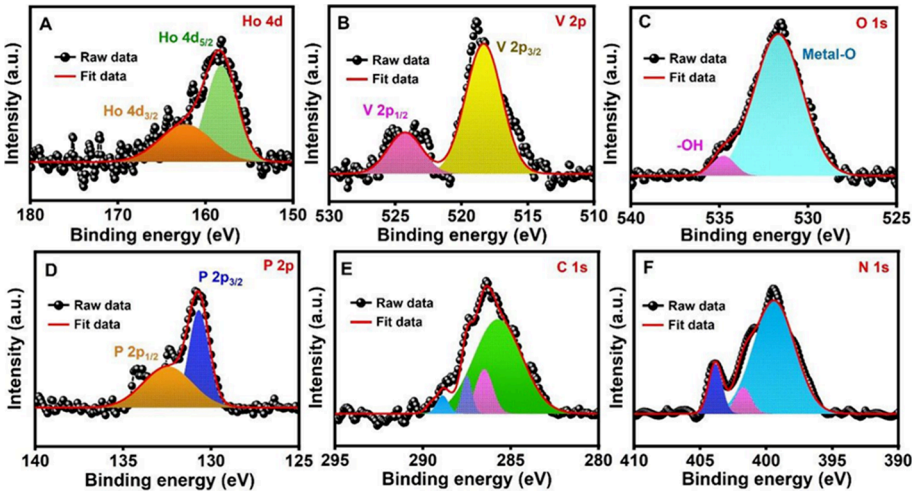

Figure 2. High-resolution XPS spectra of the $HoVO_4$/P-CN nanocomposite for (A) Ho 4d, (B) V 2p, (C) O 1s, (D) P 2p, (E) C 1s, and (F) N 1s elements.

https://doi.org/10.1021/acs.inorgchem.3c03804
Inorg. Chem. 2024, 63, 3019−3027

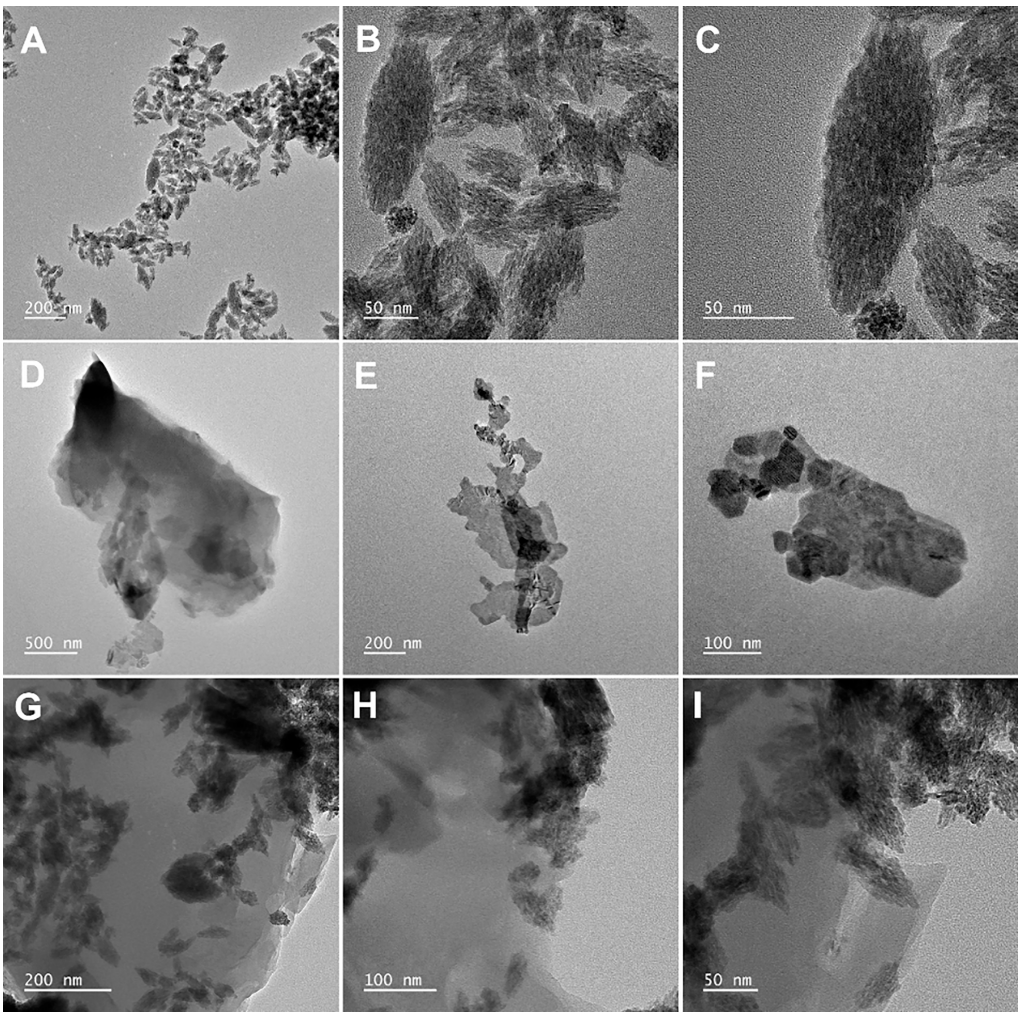

Figure 3. TEM images of the (A−C) $HoVO_4$, (D−F) P-CN, and (G−I) $HoVO_4$/P-CN nanocomposite.

Figure 2B, the peaks of V 2p at binding energies of 524.28 and 518.3 eV are indexed to V $2p_{1/2}$ and V $2p_{3/2}$ oxidation states, respectively. Figure 2C shows the O 1s XPS spectrum with peaks at 534.8 and 531.6 eV, which are attributable to vacancy oxygen (V−O) and lattice oxygen, respectively. The high-resolution spectrum of P 2p in Figure 2D can be curve-fitted with peaks at 132.54 and 130.72 eV corresponding to P−O and P−N/P−O−H, respectively. This result indicates the replacement of carbon atoms by phosphorus atoms and the formation of covalent bonds with nitrogen atoms adjacent to the heptazine unit.[50] The high-resolution C 1s XPS spectrum in Figure 2E is fitted into four peaks at 288.8, 287.5, 286.5, and 285.7 eV, corresponding to the chemical bonds of C═N, N_2−C═ N, C−N−C, and C−N, respectively. The high-resolution XPS spectrum of N 1s in Figure 2F displays peaks at 409.85, 401.74, and 399.43 eV, which correspond to N−(C_3), −N−P−, and N−C, respectively. These XPS analysis results confirm that $HoVO_4$ and P-CN are successfully combined by chemical interaction.

Transmission electron microscopy (TEM) is used for observing the morphologies of $HoVO_4$, P-CN, and HoVO4/P-CN. Figure 3A−C shows that the prepared $HoVO_4$ has a nanorice morphology with abundant interior cavities and a length of 50 to hundreds of nanometers in range. The $HoVO_4$ nanostructure possesses a surface with more active sites to promote electrochemical performance. In Figure 3D−F, the morphology of P-CN displays an ultrathin two-dimensional (2D) nanosheet-like structure. The P-CN has a 2D network structure that can enhance the mass transfer process and provide large-scale specific surface areas to ensure good dispersion of active sites. The TEM images of the $HoVO_4$/P-CN nanocomposite in Figure 3G−I show that $HoVO_4$ nanorices are covered on ultrathin P-CN nanosheets, and the loading of P-CN does not affect the distribution and orientation of $HoVO_4$. The HAADF-STEM image in Figure S2A shows that the well-dispersed $HoVO_4$ nanorices are tightly anchored onto the P-CN nanosheets. The energy-dispersive spectroscopy (EDS) spectrum in Figure S2B indicates the existence of holmium (Ho), vanadium (V), oxygen (O), phosphorus (P), carbon (C), and nitrogen (N) elements in the $HoVO_4$/P-CN nanocomposite. The elemental mapping images in Figure S2C−H clearly demonstrate the corresponding distribution of Ho, V, and O elements in $HoVO_4$ nanorices and the P, C, and N elements in P-CN nanosheets. The above physical characterization results confirm the successful preparation of the $HoVO_4$/P-CN nanocomposite without any impurity.

3.2. Electrochemical Measurement. *3.2.1. Electrochemical Properties of Unmodified and Modified Electrodes.* The interfacial charge transfer properties of various modified electrodes are evaluated through electrochemical impedance spectroscopy (EIS).[27] Figure 4A shows the Nyquist plots of

https://doi.org/10.1021/acs.inorgchem.3c03804
Inorg. Chem. 2024, 63, 3019−3027

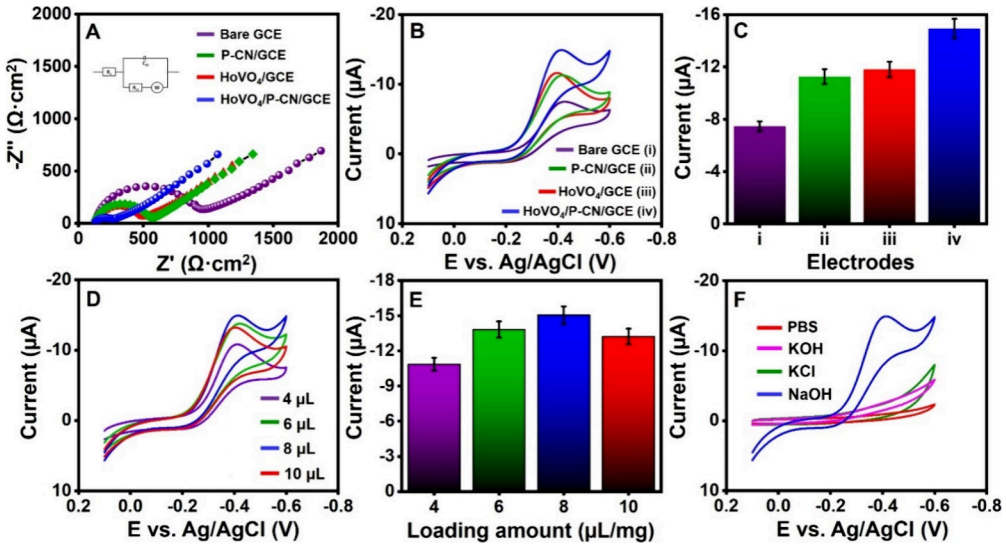

Figure 4. (A) Nyquist plots of different electrodes (inset: Randle's equivalent circuit model). (B) CV curves of 90 μM H_2O_2 in 0.1 M NaOH on different electrodes at a scan rate of 50 mV/s. (C) Comparison of reduction current for different electrodes. (D) CV curves of 90 μM H_2O_2 on the $HoVO_4$/P-CN/GCE prepared with different loading amounts of the $HoVO_4$/P-CN nanocomposite. (E) Dependence of reduction current on the loading amount. (F) CV curves of 90 μM H_2O_2 in different electrolytes on the $HoVO_4$/P-CN/GCE.

the bare GCE, $HoVO_4$/GCE, P-CN/GCE, and $HoVO_4$/P-CN/GCE in a 0.1 M KCl solution, which contains 5 mM $[Fe(CN)_6]^{3-/4-}$. These Nyquist plots are fitted using Randle's equivalent circuit model shown in the inset of Figure 4A. Randle's equivalent circuit model consists of charge transfer resistance (R_{ct}), solution resistance (R_s), double-layer capacitance (C_{dl}), and Warburg impedance (Z_w). The R_{ct} value of the electrode surface is reflected in the semicircular diameter in the Nyquist plot. The equivalent circuit calculation shows that the R_{ct} values of bare GCE, P-CN/GCE, $HoVO_4$/GCE, and $HoVO_4$/P-CN/GCE are 831, 447, 330, and 157 Ω, respectively. The $HoVO_4$/P-CN/GCE possesses the lowest R_{ct} value, which indicates the fastest electron transfer, the best conductivity, and excellent catalytic ability among all electrodes. Therefore, $HoVO_4$/P-CN/GCE is desirable for further electrochemical investigation toward H_2O_2 detection.

3.2.2. Electrochemical Sensing of H_2O_2. The cyclic voltammetry (CV) method is used to evaluate the electrochemical behavior of different electrodes. Figure 4B illustrates the CV comparison of nonenzymatic analysis of 90 μM H_2O_2 in 0.1 M NaOH on the bare GCE, $HoVO_4$/GCE, P-CN/GCE, and $HoVO_4$/P-CN/GCE at a scan rate of 50 mV/s. The CV curve of $HoVO_4$/P-CN/GCE exhibits a distinct reduction response of H_2O_2 with the lowest peak potential of −0.412 V (vs Ag/AgCl) compared to other electrodes, such as the bare GCE, $HoVO_4$/GCE, and P-CN/GCE. Notably, no oxidation peak occurs during the electrochemical reaction, suggesting an irreversible reduction process. Based on the above experimental results, a possible electrochemical reaction mechanism of H_2O_2 on $HoVO_4$/P-CN/GCE is shown in Figure S3A. The high electrocatalytic activity of the $HoVO_4$/P-CN nanocomposite might be mainly attributed to the high effective surface area, good chemical stability, high electronic conductivity, synergistic effect, unique morphology, enhanced electron transfer, and abundant electroactive sites. The reduction currents for the $HoVO_4$/P-CN/GCE are 1.26-, 1.32-, and 2-fold greater than those for the P-CN/GCE, $HoVO_4$/GCE, and bare GCE, respectively. Figure 4C displays the bar diagram of the reduction current of different electrodes. Thus, $HoVO_4$/P-CN/GCE with the highest current response and the lowest peak potential is selected for further electrochemical analysis of H_2O_2.

3.2.3. Influences of the Loading Amount and Supporting Electrolyte. The optimal loading amount of the $HoVO_4$/P-CN nanocomposite on the GCE is essential for enhancing the electrochemical reaction for H_2O_2 detection. In this study, the $HoVO_4$/P-CN/GCEs prepared with volumes of $HoVO_4$/P-CN suspension of 4, 6, 8, and 10 μL were examined by the CV method in the presence of 90 μM H_2O_2, as shown in Figure 4D,E. When the $HoVO_4$/P-CN's loading amount increases from 4 to 8 μL, the current response initially increases and achieves the maximum value at 8 μL. The further increase in the loading amount to 10 μL results in the decreased peak reduction current due to high mass transfer resistance. Therefore, 8 μL of the $HoVO_4$/P-CN suspension is the optimized loading amount on the surface of the GCE for electrochemical detection of H_2O_2. The impact of the supporting electrolytes on the electrochemical reaction of 90 μM H_2O_2 on $HoVO_4$/P-CN/GCE is shown in Figure 4F. The studied 0.1 M supporting electrolytes include PB solution, potassium hydroxide (KOH) solution, potassium chloride (KCl) solution, and sodium hydroxide (NaOH) solution. The electrochemical results show that the best electrochemical response is obtained for the NaOH solution. Thus, the NaOH solution is chosen as the supporting electrolyte in the subsequent electrochemical experiments for H_2O_2 detection.

3.2.4. Influence of the Concentration and Scan Rate. The CV response of various concentrations of H_2O_2 on the $HoVO_4$/P-CN/GCE is shown in Figure S3B. The peak reduction current increases significantly as the H_2O_2 concentration grows from 10 to 90 μM. A good linear relationship between the peak reduction current and the H_2O_2 concentration is found in Figure S3C. The linear regression equation is described as I_{pc} (μA) = −0.0809 [H_2O_2] (μM) − 7.6836 with a correlation coefficient of 0.994. These results demonstrate excellent electrocatalytic detection ability toward H_2O_2 by using the $HoVO_4$/P-CN-modified electrode. The electrochemical reduction response of 90 μM H_2O_2 on the

https://doi.org/10.1021/acs.inorgchem.3c03804
Inorg. Chem. 2024, 63, 3019−3027

$HoVO_4$/P-CN/GCE at different scan rates is explored by the CV method, as shown in Figure S3D. The peak reduction current increases gradually with the scan rate in the range from 0.02 to 0.2 V/s. Figure S3E shows that the peak reduction current linearly increases with the square root of the scan rate. The linear regression equation is described as I_{pc} (μA) = −21.036 [scan rate (V/s)]$^{1/2}$ − 9.0267 with a correlation coefficient of 0.992. These results demonstrate that the electrocatalytic reduction behavior of H_2O_2 on the surface of $HoVO_4$/P-CN/GCE is a diffusion-controlled process.

3.2.5. Analytical Performance. The amperometric method is used to investigate the analytical performance of $HoVO_4$/P-CN/GCE for H_2O_2 detection by the consecutive addition of various concentrations of H_2O_2 under continuous stirring. It is noted from Figure 5A that the reduction current rises with the

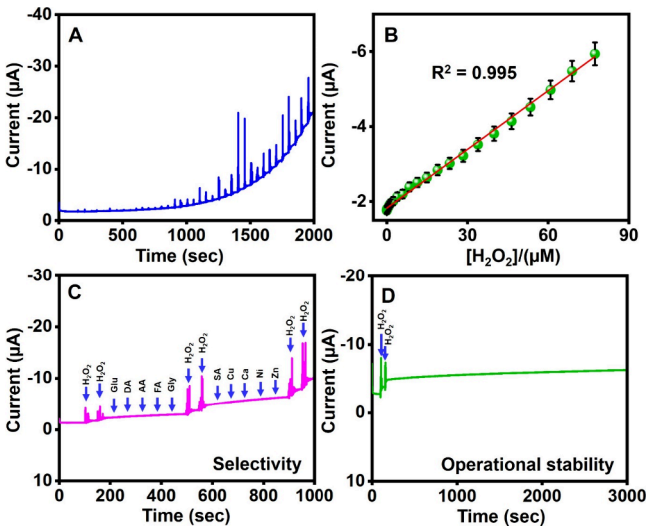

Figure 5. (A) Amperometric response of $HoVO_4$/P-CN/GCE for the successive addition of different concentrations of H_2O_2 in 0.1 M NaOH. (B) Dependence of the peak current on the H_2O_2 concentration. (C) Amperometric response of $HoVO_4$/P-CN/GCE for the addition of H_2O_2 with the presence of various interfering compounds. (D) Operational stability test of $HoVO_4$/P-CN/GCE for the detection of 30 μM H_2O_2.

H_2O_2 concentration in the stair-step way and achieves the steady-state current within 3 s. Figure 5B shows that the reduction current has a good linear relationship with the H_2O_2 concentration in the range from 0.009 to 77.4 μM. The fitting linear regression equation is I_{pc} (μA) = −0.0504 [H_2O_2](μM) − 1.8432 with a correlation coefficient of 0.995. The LOD and the sensitivity of $HoVO_4$/P-CN/GCE are calculated as 0.003 μM and 0.72 μA μM^{-1} cm^{-2}, respectively. The analytical performance of the proposed $HoVO_4$/P-CN-modified GCE for H_2O_2 detection is compared to the previous reports in Table 1.[11,51−60] This analytical study reveals that the proposed $HoVO_4$/P-CN nanocomposite-based electrochemical sensor shows superior or equivalent sensing performance for H_2O_2 detection compared with the formerly reported electrochemical platforms. The superior electrochemical performance of the $HoVO_4$/P-CN nanocomposite is attributed to good electrical conductivity, synergistic effect, large surface area, and more active sites. Therefore, the $HoVO_4$/P-CN nanocomposite-modified GCE can be utilized in an actual sample analysis.

Table 1. Performance Comparison of Various Electrode Materials for H_2O_2 Detection.

electrode material	linear range (μM)	LOD (μM)	ref.
CuO-CeO_2/MXene	5−100	1.7	11
ERGO	1−16	0.7	51
Ag−Au NPs	30−300	0.18	52
Pd NP	0.1−1.8	0.04	53
hemin/PA-PANI	2−102	1.2	54
Fe_3O_4@Ag	0.5−20	0.16	55
Ag−TiN	0.2−220	0.02	56
CuO/g-C_3N_4	0.5−50	0.31	57
Pt_rGO@PILs	2.3−250	1.5	58
Nb_2CT_x/PB	1−10	0.2	59
	10−100		
Fe_3O_4/Gr	10−110	4.79	60
$HoVO_4$/P-CN	0.009−77.4	0.003	this work

3.2.6. Selectivity, Stability, Repeatability, and Reproducibility. Selectivity is essential in evaluating electrochemical sensors for H_2O_2 detection in practical applications. For this reason, the effect of other potentially similar or interfering compounds that might coexist in the actual samples containing H_2O_2 was examined. The selectivity of the $HoVO_4$/P-CN-modified GCE is investigated by the amperometric method for the detection of 30 μM H_2O_2 with the continuous addition of various interfering compounds. The studied interfering compounds include the 100-fold excess amount of glucose (Glu), dopamine (DA), ascorbic acid (AA), folic acid (FA), glycine (Gly), and salicylic acid (SA) and the 200-fold excess amount of copper (Cu), calcium (Ca), nickel (Ni), and zinc (Zn). The current response shown in Figure 5C shows that the existence of potentially interfering compounds does not noticeably affect the reduction current produced by the $HoVO_4$/P-CN-based electrochemical sensor. The above results indicate that the proposed $HoVO_4$/P-CN/GCE exhibits a high selectivity for determining H_2O_2.

The operational stability of $HoVO_4$/P-CN/GCE is investigated by the amperometry method. The investigation of Figure 5D shows that the current response for 30 μM H_2O_2 can remain at 94% of its original response after 3000 s, which reveals the preferable operational stability of the proposed $HoVO_4$/P-CN sensor. Figure S4A shows the repeatability test of $HoVO_4$/P-CN/GCE for the detection of 90 μM H_2O_2 under the same condition mentioned in Section 3.2.2. The histogram of peak current for four $HoVO_4$/P-CN-based H_2O_2 sensors is shown in Figure S4B. The relative standard deviation (RSD) value of the peak current is 0.313%, indicating that the $HoVO_4$/P-CN-modified GCE has good repeatability for H_2O_2 detection. The reproducibility of the proposed sensor is evaluated by detecting 90 μM H_2O_2 on three $HoVO_4$/P-CN-based sensors under the same condition, as depicted in Figure S4C. The peak current histogram of the three $HoVO_4$/P-CN-based sensors is shown in Figure S4D. The CV analysis results show an RSD value of 0.8%, which confirms that the $HoVO_4$/P-CN-based sensor has good reproducibility for H_2O_2 detection. These results indicate satisfactory selectivity, stability, repeatability, and reproducibility of the $HoVO_4$/P-CN-based electrochemical sensor for H_2O_2 sensing.

3.2.7. Practical Application. The practicability of $HoVO_4$/P-CN/GCE was investigated by the determination of H_2O_2 in real samples. The sample for milk was purchased from a local shop in Taipei, Taiwan. The sample for human urine was

https://doi.org/10.1021/acs.inorgchem.3c03804
Inorg. Chem. 2024, 63, 3019−3027

collected from a healthy volunteering person. These H_2O_2 free real samples were centrifuged and diluted with DI water. Then, both samples were spiked with the H_2O_2 solution according to the standard addition method. The amperometry response of $HoVO_4$/P-CN/GCE in Figure S5A,B displays a robust and good current change for the detection of H_2O_2 in milk and human urine. The reliability of the proposed H_2O_2 sensor based on the $HoVO_4$/P-CN nanocomposite was evaluated using the high-performance liquid chromatography (HPLC) method. The recovery values measured by the proposed electrochemical method and the HPLC method are given in Table S1 for comparison. The recovery values for milk and human urine samples measured by the proposed electrochemical sensor are in the range of 96.7−98.75%, which is close to the range (97.3−98.6%) measured by the HPLC analysis. This indicates that the proposed $HoVO_4$/P-CN nanocomposite-based electrochemical sensor has good accuracy and satisfactory reliability for the detection of H_2O_2 in the actual samples.

4. CONCLUSIONS

We present the synthesis of $HoVO_4$/P-CN nanocomposites as an efficient electrocatalyst for nonenzymatic electrochemical H_2O_2 detection by attaching the hydrothermally synthesized $HoVO_4$ nanorices on ultrathin P-CN nanosheets. Various analytical methods, such as XRD, FTIR, XPS, TEM, EDS, and elemental mapping, are used to confirm the successful formation of the $HoVO_4$/P-CN nanocomposites. The $HoVO_4$/P-CN-modified GCE exhibits superior electrochemical sensing capability toward H_2O_2 reduction compared to the bare GCE, $HoVO_4$-modified GCE, and P-CN-modified GCE. The excellent detection performance of the proposed H_2O_2 sensor includes the wide linear working range of 0.009−77.4 μM, ultralow LOD of 3 nM, and high sensitivity of 0.72 μA μM^{-1} cm^{-2}. In addition, the $HoVO_4$/P-CN-modified GCE exhibits satisfactory stability, repeatability, and reproducibility. Importantly, the $HoVO_4$/P-CN-modified GCE has high selectivity in the presence of various potential interfering compounds in real-world samples, such as milk and human urine. The proposed electrochemical sensor based on $HoVO_4$/P-CN nanocomposites presents great promise for nonenzymatic sensing of H_2O_2 in the fields of food safety and clinical diagnostics.

■ ASSOCIATED CONTENT

Supporting Information

The Supporting Information is available free of charge at https://pubs.acs.org/doi/10.1021/acs.inorgchem.3c03804.

Materials, instrumentation, synthesis of $HoVO_4$ nanorices, synthesis of P-CN nanosheets, XPS survey spectrum, HAADF-STEM image, EDS spectrum, elemental mapping images, electrochemical reduction mechanism of H_2O_2, CV curves of different concentrations of H_2O_2 on the $HoVO_4$/P-CN/GCE, dependence of peak current on the H_2O_2 concentration, CV response of 90 μM H_2O_2 on the $HoVO_4$/P-CN/GCE at different scan rates, dependence of peak current on the square root of scan rates, repeatability test, reproducibility test, amperometric response for the addition of H_2O_2 in milk and human urine samples, and recovery measurement result (PDF)

■ AUTHOR INFORMATION

Corresponding Author

Tzyy-Jiann Wang − *Department of Electro-Optical Engineering, National Taipei University of Technology, Taipei 106, Taiwan;* orcid.org/0000-0002-0668-4728; Email: f10939@ntut.edu.tw

Authors

Thangavelu Kokulnathan − *Department of Electro-Optical Engineering, National Taipei University of Technology, Taipei 106, Taiwan;* orcid.org/0000-0002-2354-6327

Faheem Ahmed − *Department of Applied Sciences & Humanities, Faculty of Engineering & Technology, Jamia Millia Islamia, New Delhi 110025, India*

Thamraa Alshahrani − *Department of Physics, College of Science, Princess Nourah bint Abdulrahman University, Riyadh 11671, Saudi Arabia*

Nishat Arshi − *Department of Basic Sciences, Preparatory Year Deanship, King Faisal University, Al-Ahsa 31982, Saudi Arabia*

Complete contact information is available at: https://pubs.acs.org/10.1021/acs.inorgchem.3c03804

Notes

The authors declare no competing financial interest.

■ ACKNOWLEDGMENTS

The authors gratefully acknowledge the financial support of the Ministry of Science and Technology of Taiwan through grant numbers MOST 111-2221-E-027-020-MY3 and MOST 111-2221-E-027-085 and the Princess Nourah bint Abdulrahman University Researchers through supporting project number PNURSP2023R1, Princess Nourah bint Abdulrahman University, Riyadh, Saudi Arabia.

■ REFERENCES

(1) Kou, M.; Wang, Y.; Xu, Y.; Ye, L.; Huang, Y.; Jia, B.; Li, H.; Ren, J.; Deng, Y.; Chen, J.; Zhou, Y.; Lei, K.; Wang, L.; Liu, W.; Huang, H.; Ma, T. Molecularly engineered covalent organic frameworks for hydrogen peroxide photosynthesis. *Angew. Chem., Int. Ed.* **2022**, *61* (19), No. e202200413.

(2) Liu, J.; Li, X.; Cheng, L.; Sun, J.; Xia, X.; Zhang, X.; Song, Y.; Sun, D.; Sun, J.; Zhang, L. Atomic layer deposition of Pt nanoparticles onto Co/MoN nanoarrays for improved electrochemical detection of H_2O_2. *Chem. Commun.* **2023**, *59* (4), 474−477.

(3) Giaretta, J. E.; Duan, H.; Oveissi, F.; Farajikhah, S.; Dehghani, F.; Naficy, S. Flexible sensors for hydrogen peroxide detection: A critical review. *ACS Appl. Mater. Interfaces* **2022**, *14* (18), 20491−20505.

(4) Baye, A. F.; Thi Nguyen, H.; Kim, H. Fe0/Fe_3C-assisted Fe_3O_4 redox sites as robust peroxidase mimics for colorimetric detection of H_2O_2. *Sens. Actuators, B* **2023**, *377*, No. 133097.

(5) Zhao, W.; Yan, P.; Li, B.; Bahri, M.; Liu, L.; Zhou, X.; Clowes, R.; Browning, N. D.; Wu, Y.; Ward, J. W.; Cooper, A. I. Accelerated synthesis and discovery of covalent organic framework photocatalysts for hydrogen peroxide production. *J. Am. Chem. Soc.* **2022**, *144* (22), 9902−9909.

(6) Xing, L.; Zhang, W.; Fu, L.; Lorenzo, J. M.; Hao, Y. Fabrication and application of electrochemical sensor for analyzing hydrogen peroxide in food system and biological samples. *Food Chem.* **2022**, No. 132555.

(7) Zhang, Y.; Sun, Q.; Guo, G.; Cheng, Y.; Zhang, X.; Ji, H.; He, X. Trace Pt atoms as electronic promoters in Pd clusters for direct synthesis of hydrogen peroxide. *Chemical Engineering Journal* **2023**, *451*, No. 138867.

(8) Zhang, D.; Mitchell, E.; Lu, X.; Chu, D.; Shang, L.; Zhang, T.; Amal, R.; Han, Z. Metal-free carbon-based catalysts design for oxygen reduction reaction towards hydrogen peroxide: From 3D to 0D. *Materials Today.* **2023**, *63*, 339−359.
(9) Jia, Y.; Bai, Y.; Chang, J.; Zhai, Y.; Zhang, T.; Ren, K.; Hong, J. Life cycle assessment of hydrogen peroxide produced from mainstream hydrogen sources in China. *Journal of Cleaner Production* **2022**, *352*, No. 131655.
(10) Yang, B.; Wang, K.; Zhou, J.; Shao, X.; Gu, X.; Xue, Y.; Tian, S. Ratiometric SERS detection of H_2O_2 and glucose using a pyrroloquinoline skeleton containing molecule as H_2O_2-responsive probe. *Appl. Surf. Sci.* **2022**, *590*, No. 153020.
(11) Zhou, K.; Li, Y.; Zhuang, S.; Ren, J.; Tang, F.; Mu, J.; Wang, P. A novel electrochemical sensor based on CuO-CeO_2/MXene nanocomposite for quantitative and continuous detection of H_2O_2. *J. Electroanal. Chem.* **2022**, *921*, No. 116655.
(12) Xia, C.; He, W.; Yang, X. F.; Gao, P. F.; Zhen, S. J.; Li, Y. F.; Huang, C. Z. Plasmonic hot-electron-painted Au@Pt nanoparticles as efficient electrocatalysts for detection of H_2O_2. *Anal. Chem.* **2022**, *94* (39), 13440−13446.
(13) Mohiuddin, A. K.; Jeon, S. Highly efficient Ag doped δ-MnO_2 decorated graphene: Comparison and application in electrochemical detection of H2O2. *Appl. Surf. Sci.* **2022**, *592*, No. 153162.
(14) Li, J.; Wu, C.; Yuan, C.; Shi, Z.; Zhang, K.; Zou, Z.; Xiong, L.; Chen, J.; Jiang, Y.; Sun, W.; Tang, K.; Yang, H.; Li, C. M. Single-atom iron anchored on 2-D graphene carbon to realize bridge-adsorption of O−O as biomimetic enzyme for remarkably sensitive electrochemical detection of H_2O_2. *Anal. Chem.* **2022**, *94* (41), 14109−14117.
(15) Luo, S.; Kan, X. Specifically triggered dissociation based ratiometric electrochemical sensor for H_2O_2 measurement in food samples. *Food Chem.* **2022**, *387*, No. 132922.
(16) Wang, L.; Li, Y.; Zhang, C.; Deng, D.; He, H.; Yan, X.; Li, Z.; Luo, L. Hierarchical NiMn layered double hydroxide nanostructures on carbon cloth for electrochemical detection of hydrogen peroxide. *ACS Applied Nano Materials* **2022**, *5* (12), 17741−17749.
(17) Wang, M.; Qiu, S.; Yang, H.; Huang, Y.; Dai, L.; Zhang, B.; Zou, J. Spectrophotometric determination of hydrogen peroxide in water with peroxidase-catalyzed oxidation of potassium iodide and its applications to hydroxylamine-involved Fenton and Fenton-like systems. *Chemosphere* **2021**, *270*, No. 129448.
(18) Li, L.; Zheng, M.; Yan, X.; Huang, H.; Cao, S.; Liu, K.; Liu, J. B. Quantitative detection of H_2O_2 with a composite fluorescent probe of 8-quinoline boronic acid-Al (III). *J. Photochem. Photobiol., A* **2022**, *432*, No. 114069.
(19) Wang, K.; Liu, Y.; Li, D.; Zhang, A.; Mo, P.; Liu, J.; Wang, Y.; Chen, Y. Electrodeposited alginate- based green synthesis of CuS nanoparticles and nanocomposite films for electrochemical and colorimetric detection. *Macromol. Mater. Eng.* **2022**, *307* (8), 2200090.
(20) Rong, X.; Liu, W.; Wang, X.; Li, M.; Wang, J.; Lin, Z.; Yan, J.; Yuan, Y. A photoelectrochemical sensor for highly sensitive detection of H_2O_2 based on [Fcmim][N $(CN)_2$]@ Nafion® film modified GaN through a parallel catalysis strategy. *Sens. Actuators, B* **2022**, *365*, No. 131914.
(21) Sohrabi, H.; Maleki, F.; Khaaki, P.; Kadhom, M.; Kudaibergenov, N.; Khataee, A. Electrochemical-based sensing platforms for detection of glucose and H_2O_2 by porous metal−organic frameworks: A review of status and prospects. *Biosensors* **2023**, *13* (3), 347.
(22) Xiao, C.; Izquierdo-Roca, V.; Rivera-Gil, P. Real time and spatiotemporal quantification of pH and H_2O_2 imbalances with a multiplex surface-enhanced raman spectroscopy nanosensor. *ACS Materials Au.* **2023**, *3* (2), 164−175.
(23) Wang, C.; Wang, Y.; Wang, G.; Huang, C.; Jia, N. A new mitochondria-targeting fluorescent probe for ratiometric detection of H_2O_2 in live cells. *Anal. Chim. Acta* **2020**, *1097*, 230−237.
(24) Santhan, A.; Hwa, K. Y. Facile synthesis of needle-like copper sulfide structures as an effective electrochemical sensor material for neurotransmitter detection in biological samples. *Sensors* **2023**, *23* (21), 8849.
(25) Kaleeswarran, P.; Sakthi Priya, T.; Chen, T. W.; Chen, S. M.; Kokulnathan, T.; Arumugam, A. Construction of a copper bismuthate/graphene nanocomposite for electrochemical detection of catechol. *Langmuir* **2022**, *38* (33), 10162−10172.
(26) Kong, D. R.; Xin, Y. Y.; Zhang, X. F.; Deng, Z. P.; Huo, L. H.; Gao, S. $CoCr_2O_4$/Graphene modified glass carbon electrode for highly dual-sensing detection of hydrogen peroxide and glucose. *Appl. Surf. Sci.* **2024**, *644*, No. 158769.
(27) Kokulnathan, T.; Wang, T. J.; Ahmed, F.; Alshahrani, T. Synthesis of 3D flower-like zinc-chromium layered double hydroxides: a functional electrode material for furaltadone detection. *Process Safety and Environmental Protection* **2023**, *176*, 889−897.
(28) Maria Stanley, M.; Sherlin V, A.; Wang, S. F.; Baby, J. N.; Sriram, B.; George, M. Deep eutectic solvent assisted synthesis of molybdenum nitride entrapped graphene aerogel heterostructure with enhanced electrochemical behavior for ronidazole drug detection. *J. Mol. Liq.* **2023**, *375*, No. 121308.
(29) Kokulnathan, T.; Vishnuraj, R.; Wang, T. J.; Pullithadathil, B.; Rangarajan, M.; Ahmed, F.; Alshahrani, T. S Strongly coupled design of zinc oxide-nanorods/copper tin sulfide-nanoflowers nanostructures: An electrochemical study in 4-nitrochlorobenzene detection. *Chemical Engineering Journal* **2024**, *479*, No. 147747.
(30) Kaplan, S.; Suna Karatekin, R.; Kahya Dudukcu, M.; Avcı, G. A novel Ni−Fe_3O_4@s-rGO/GCE electrode for electrochemical detection of H_2O_2. *Mater. Chem. Phys.* **2023**, *294*, No. 127051.
(31) Xiong, L.; Zhang, Y.; Wu, S.; Chen, F.; Lei, L.; Yu, L.; Li, C. Co_3O_4 nanoparticles uniformly dispersed in rational porous carbon nano-boxes for significantly enhanced electrocatalytic detection of H_2O_2 released from living cells. *International Journal of Molecular Sciences* **2022**, *23* (7), 3799.
(32) Rauf, S.; Mani, V.; Lahcen, A. A.; Yuvaraja, S.; Beduk, T.; Salama, K. N. Binary transition metal oxide modified laser-scribed graphene electrochemical aptasensor for the accurate and sensitive screening of acute myocardial infarction. *Electrochim. Acta* **2021**, *386*, No. 138489.
(33) Kanna Sharma, T. S.; Hwa, K. Y.; Santhan, A.; Ganguly, A. Synthesis of novel three-dimensional flower-like cerium vanadate anchored on graphitic carbon nitride as an efficient electrocatalyst for real-time monitoring of mesalazine in biological and water samples. *Sens. Actuators, B* **2021**, *331*, No. 129413.
(34) Huang, H.; Zhu, J. J. The electrochemical applications of rare earth-based nanomaterials. *Analyst* **2019**, *144* (23), 6789−6811.
(35) Tojo, T.; Zhang, Q.; Saito, F. Mechanochemical synthesis of rare earth orthovanadates from R_2O_3 (R= rare earth elements) and V_2O_5 powders. *Journal of alloys and compounds* **2007**, *427* (1−2), 219−222.
(36) Kokulnathan, T.; Chen, S. M. Robust and selective electrochemical detection of antibiotic residues: The case of integrated lutetium vanadate/graphene sheets architectures. *Journal of hazardous materials* **2020**, *384*, No. 121304.
(37) Sriram, B.; Baby, J. N.; Hsu, Y. F.; Wang, S. F.; George, M. Scheelite-type rare earth vanadates TVO_4 (T= Ho, Y, Dy) electrocatalysts: Investigation and comparison of T site variations towards bifunctional electrochemical sensing application. *Chemical Engineering Journal* **2023**, *451*, No. 138694.
(38) Alborzi, A.; Nasiri, M. Novel size-controlled fabrication of pure $HoVO_4$ nanoparticles via a new approach. *Journal of Materials Science: Materials in Electronics* **2017**, *28*, 13829−13835.
(39) Sriram, B.; Baby, J. N.; Hsu, Y. F.; Wang, S. F.; George, M. Toward the development of disposable electrodes based on holmium orthovanadate/f-boron nitride: mpacts and electrochemical performances of emerging inorganic contaminants. *Inorg. Chem.* **2021**, *60* (16), 12425−12435.
(40) Mehmandoust, M.; Erk, N.; Naser, M.; Soylak, M. Molecularly imprinted polymer film loaded on the metal−organic framework with improved performance using stabilized gold-doped graphite carbon

https://doi.org/10.1021/acs.inorgchem.3c03804
Inorg. Chem. 2024, 63, 3019−3027

nitride nanosheets for the single-step detection of fenamiphos. *Food Chem.* **2023**, *404*, No. 134627.
(41) Duraisamy, N.; Kokulnathan, T.; Kesavan, G. *Graphitic carbon nitride for electrocatalysis. Nanoscale Graphitic Carbon Nitride: Synthesis and Applications*; Elsevier: 2022, 193−224. DOI: DOI: 10.1016/B978-0-12-823034-3.00014-5.
(42) Mohammadzadeh Jahani, P.; Aflatoonian, M. R.; Abbasi Rayeni, R.; Di Bartolomeo, A.; Mohammadi, S. Z. Graphite carbon nitride-modified screen-printed electrode as a highly sensitive and selective sensor for detection of amaranth. *Food Chem. Toxicol.* **2022**, *163*, No. 112962.
(43) Hwa, K. Y.; Santhan, A.; Ganguly, A.; Kanna Sharma, T. S. Two dimensional architectures of graphitic carbon nitride with the substitution of heteroatoms for bifunctional electrochemical detection of nilutamide. *Chemosphere* **2023**, *320*, No. 138068.
(44) Umapathi, R.; Venkateswara Raju, C.; Majid Ghoreishian, S.; Mohana Rani, G.; Kumar, K.; Oh, M. H.; Pil Park, J.; Suk Huh, Y. Recent advances in the use of graphitic carbon nitride-based composites for the electrochemical detection of hazardous contaminants. *Coord. Chem. Rev.* **2022**, *470*, No. 214708.
(45) Ebrahimi, S.; Afkhami, A.; Madrakian, T.; Amouzegar, Z. Self-supporting porous S-doped graphitic carbon nitride as a multifunctional support of Au catalyst: Application to highly sensitive and selective determination of arsenic (III) in a wide range of pH. *Electrochim. Acta* **2023**, *437*, No. 141496.
(46) Sivaraman, N.; Duraisamy, V.; Lucious, L.; Saraswathyamma, B.; Kumar, S. M. S.; Thangamuthu, R. In-situ construction of N and P doped hollow sphere carbon for electrochemical sensing of antibiotic drug from poultry sustenance. *Electrochim. Acta* **2023**, *441*, No. 141773.
(47) Kokulnathan, T.; Wang, T. J. Synthesis and characterization of 3D flower-like nickel oxide entrapped on boron doped carbon nitride nanocomposite: An efficient catalyst for the electrochemical detection of nitrofurantoin. *Composites Part B: Engineering* **2019**, *174*, No. 106914.
(48) Prasanna, S. B.; Kumar, G. K. S.; Shadakshari, S.; Shivamurthy, S. A.; Shanthakumar, K. C.; Nagaraja, B. M.; Chung, R. J. Advanced sensing of antibiotics with Sr@Se flower-like structure on phosphorus-doped g-C_3N_4 composite: Application towards detection of chloramphenicol in food samples. *Chemosensors* **2022**, *10* (10), 425.
(49) Ahmed, F.; Kokulnathan, T.; Umar, A.; Akbar, S.; Kumar, S.; Shaalan, N. M.; Arshi, N.; Alam, M. G.; Aljaafari, A.; Alshoaibi, A. Zinc oxide/phosphorus-doped carbon nitride composite as potential scaffold for electrochemical detection of nitrofurantoin. *Biosensors* **2022**, *12* (10), 856.
(50) Sriram, B.; Baby, J. N.; Hsu, Y. F.; Wang, S. F.; Benadict Joseph, X.; George, M.; Veerakumar, P.; Lin, K. C. $MnCo_2O_4$ microflowers anchored on P-doped g-C_3N_4 nanosheets as an electrocatalyst for voltammetric determination of the antibiotic drug sulfadiazine. *ACS Applied Electronic Materials* **2021**, *3* (9), 3915−3926.
(51) Mutyala, S.; Mathiyarasu, J. A reagentless non-enzymatic hydrogen peroxide sensor presented using electrochemically reduced graphene oxide modified glassy carbon electrode. *Materials Science and Engineering: C* **2016**, *69*, 398−406.
(52) Zhao, L.; Song, J.; Xue, Y.; Zhao, X.; Deng, Y.; Li, Q.; Xia, Y. Green synthesis of Ag−Au bimetallic nanoparticles with alginate for sensitive detection of H_2O_2. *Catal. Lett.* **2018**, *148*, 3248−3256.
(53) Ehsan, M. A.; Hasan, M. M.; Islam, T.; Hossain, M. D.; Aziz, M. A.; Ahammad, A. S. Fabrication of nanostructured Pd thin films using aerosol-assisted chemical vapor deposition for the nonenzymatic electrochemical detection of H_2O_2. *ACS Applied Electronic Materials* **2019**, *1* (3), 417−429.
(54) Shang, X.; He, S.; Xu, Z.; Lu, W.; Zhang, W. Hemin- phytic acid functionalized porous conducting polymer hydrogel with good biocompatibility for electrochemical detection of H_2O_2 released from living cells. *Electroanalysis* **2021**, *33* (4), 1088−1095.
(55) Guo, Z.; Xu, J.; Zhang, J.; Hu, Y.; Pan, Y.; Miao, P. Facile strategy for electrochemical analysis of hydrogen peroxide based on multifunctional Fe_3O_4@Ag nanocomposites. *ACS Applied Bio Materials* **2018**, *1* (2), 367−373.
(56) Chu, Y.; Zhang, H.; Zhou, H.; Xu, T.; Yan, H.; Huang, Z.; Zhao, F. L-tyrosine-assisted synthesis of nanosilver/titanium nitride with hollow microsphere structure for electrochemical detection of hydrogen peroxide. *J. Solid State Electrochem.* **2023**, *27* (3), 753−761.
(57) Atacan, K.; Özacar, M. Construction of a non-enzymatic electrochemical sensor based on CuO/g-C_3N_4 composite for selective detection of hydrogen peroxide. *Mater. Chem. Phys.* **2021**, *266*, No. 124527.
(58) Shekh, M. I.; Lu, T.; Kumar, A.; Sharma, G.; Zhu, G.; Stadler, F. J.; Du, B. Facile microwave-assisted synthesis of Pt single atom anchored on poly (ionic liquids) functionalized reduced graphene oxide for ultrasensitive detection of H_2O_2. *Journal of Environmental Chemical Engineering* **2023**, *11*, No. 110238.
(59) Mohan Arjun, A.; Shabana, N.; Ankitha, M.; Abdul Rasheed, P. Electrochemical deposition of Prussian blue on Nb_2CT_x MXene modified carbon cloth for the non-enzymatic electrochemical detection of hydrogen peroxide. *Microchem. J.* **2023**, *185*, No. 108301.
(60) Sobahi, N.; Imran, M.; Khan, M. E.; Mohammad, A.; Alam, M. M.; Yoon, T.; Mehedi, I. M.; Hussain, M. A.; Abdulaal, M. J.; Jiman, A. A. Electrochemical sensing of H_2O_2 by employing a flexible Fe_3O_4/graphene/carbon cloth as working electrode. *Materials* **2023**, *16* (7), 2770.

https://doi.org/10.1021/acs.inorgchem.3c03804
Inorg. Chem. 2024, 63, 3019−3027